Ref. Ares(2023)8808113 - 21/12/2023

HEATERNAL

Deliverable D3.1

Refractory materials and PCMs selection

Due date of deliverable: 31.12.2023
Actual submission date: 21.12.2023

Responsible WP3: CIC energiGUNE
Task Leader: CIC energiGUNE
Revision: v2.0

Funded by the European Union

Document Control Sheet

PROJECT INFORMATION

Project Number	101103921		
Project Acronym	HEATERNAL		
Project Full title	innovative High tEmperAture ThErmal stoRage for iNdustrial AppLications		
Project Start Date	01/05/2023		
Project Duration	42 months		
Funding Instrument	Horizon Europe	Funding Scheme	HORIZON-CL5-2022-D4-01-05
Topic	Development of high temperature thermal storage for industrial applications		
Coordinator	CEA		

DELIVERABLE INFORMATION

Deliverable No	**3.1**
Deliverable Title	**Refractory materials and PCMs selection**
Work-Package No	3
Work-Package Title	Storage materials development
WP-Leader (Name and Short Org. Name)	CIC energiGUNE (CICe)
Task No	3.1
Task Title	Materials selection
Task Leader (Name and Short Org. Name)	CICe
Main Author (Name and Short Org. Name)	Kyran Williamson (CICe), Ángel Serrano (CICe)
Other Authors (Name and Short Org. Name)	Bertrand Hiot (Calderys), Elena Palomo del Barrio (CICe), Grégory Largiller (CEA), Laura Teodorescu (CEA), Paola Crocomo (CICe), Artem Nikulin (CICe)
Reviewers (Name and Short Org. Name)	
Status	Draft ☐ Final ☒
Deliverable Type	Report ☒ Data ☐ Demonstration ☐ Other ☐
Dissemination Level	Public (PU) ☒ Sensitive (SEN) ☐ Classified ☐ PU: Public, fully open SEN: Sensitive, limited under the conditions of the Grant Agreement Classified R-UE/EU-R – EU RESTRICTED under the Commission Decision No2015/444 Classified C-UE/EU-C – EU CONFIDENTIAL under the Commission Decision No2015/444 Classified S-UE/EU-S – EU SECRET under the Commission Decision No2015/444
Date Approved by Coordinator	20/12/2023

DOCUMENT VERSION HISTORY

Version	Date	Author	Description of Change
V1.0	13-11-2023	Angel Serrano (CICe)	Composed draft document
V1.1	13-11-2023	Bertrand Hiot (CALD)	Refractory materials section added
V1.2	22-11-2023	Kyran Williamson (CICe)	Added in results for 4.1 Alloy selection
V1.3	30-11-2023	Carlos Concepcion (TCID)	Review of document and general comments.
V1.4	11-12-2023	Laura Teodorescu (CEA)	Added literature review and CEA results.
V1.5	12-12-2023	Kyran Williamson (CICe)	Corrections
V2.0	14-12-2023	Ángel Serrano (CICe)	Final corrections

DOCUMENT REVIEW

Reviewer	Date	Reviewer Name (Short Organisation Name)
Project Manager	18/12/2023	Claire Houzé (CEA)
Exploitation Manager	20/12/2023	Ana Fernandes (SPI)
Coordinator	20/12/2023	Sylvie Douard (CEA)

Legal disclaimer

This project has received funding from the European Union's Horizon Europe research and innovation program under grant agreement No. 101103921

ABBREVIATIONS

Abbreviation	Definition
TES	Thermal energy storage
TESS	Thermal energy storage system
HTF	Heat transfer fluid
PCM	Phase change material
CRM	Critical raw material
CAPEX	Capital expenditure
OPEX	Operating expenditure
MRL	Manufacturing readiness level
CALPHAD	Computer Coupling of Phase Diagrams and Thermochemistry
SEM-EDX	Scanning electron microscopy - Energy Dispersive Spectrometer
STA	Simultaneous thermal analysis
CTE	Coefficient of thermal expansion
TGA	Thermogravimetric analysis
DSC	Differential scanning calorimetry

Table of contents

Index of figures

Index of tables

Executive Summary

HEATERNAL develops a Thermal Energy Storage (TES) System (TESS) conceived to meet industry needs of constant high temperature heat in the face of climate and geopolitical urgencies.

HEATERNAL's TESS will recover industrial waste heat or renewable energy to replace natural gas. The consortium gathers 4 energy-intensive European industries from aluminium, ceramics and steel, an engineering/thermal-equipment manufacturer and leading research teams in energy storage, materials, modelling, system design, prototyping, LCA, techno-economic assessment and technology transfer to industry.

The TESS will be designed to satisfy the thermal energy requirements from 3 use-cases:

1. TES for the aluminium industry [ALCOA]: Store renewable energy as high-temperature heat in an alumina refinery.
2. TES for ceramic pigment furnaces [TCID]: Waste heat from a continuous process (smelters) will be stored and reused in a batch process (ceramic pigment furnace) to preheat air between 650 and 900 ºC.
3. TES for steel furnace [UGIT]: Store industrial waste heat to operate a steel furnace during natural gas shortages and cut-offs. The solution will maintain temperature to prevent material damage due to thermal shocks.

HEATERNAL CONCEPT is made of a refractory brick containing phase-change materials (PCMs). The TESS contains 3 zones with 3 different PCMs in refractory bricks, each undergoing phase changes at a different temperature. With this concept, HEATERNAL´s ambition is to achieve: 1. Optimized cost-effective system; 2. Lifetime >10 years; 3. Manufacturability for rapid market entry; 4. To ensure market entry by 2030 and 10% market share by 2040.

WP3 aims to develop and characterize the core element of the TESS: ceramic/PCM composites for TES at 600-900 ºC following defined KPIs. This involves the selection of candidate ceramic blends and PCMs considering target KPIs (T3.1).

The development of WP3 directly contributes to achieving OBJ#1, to maximize the thermal properties of the TESS, as well as OBJ#4, to ensure the reliability of the thermal storage unit from 600-900ºC.

1. Introduction

The HEATERNAL thermal energy storage system **(**TESS) combines refractory materials and PCMs to achieve both sensible and latent heat storage. To optimize efficiency and stability through repeated cycles, HEATERNAL will investigate compatible combinations considering existing ceramic formulations intended for use with metal alloys.

The primary goal of HEATERNAL is to:

Design a cost-efficient TESS consisting of hollow ceramic refractory bricks partially filled with Phase Change Materials (PCMs).

Specific geometries (shape, size, and void space) will be developed which will optimize the flow of a heat transfer fluid (HTF). Thermal properties and compatibility with MRL9-10 manufacturing technologies, specifically uniaxial compression with moulds will be utilised. Simultaneously, in anticipation of the growing use of 3D printing in ceramic composite manufacturing, HETERNAL aims to explore innovative unit designs that leverage the advantages of 3D printing, offering improved thermal properties compared to traditional mould techniques.

The objective of this deliverable (D3.1) is to:

Report on a preliminary selection of stable ceramic materials and PCM composite materials for operating temperature of 600 °C - 900 °C.

The selection will be based on the following key performance indicators (KPIs): Heat storage capacity > 400 kWh/m^3; Proven lifetime > 1000 hours; Low energy & CO_2 footprint; Non-toxic and safe, and easy to recycle.

All these requirements are gathered and defined in detail in D2.1 (WP2*)*. In addition, the definition of the demo cases KPIs and process parameters establish the required temperatures for the TESS.

Task 3.1 will provide a short list of possible refractory chemistries/PCM combinations considering not only cost and storage performance but also compatibility issues. Two families of promising PCMs for high-temperature (600 – 900 °C) heat storage will be considered:

1. **Metal alloy PCMs, undergoing solid-liquid phase transitions (Al-alloys and Cu-alloys)**
2. **Sulphate based PCMs (SS-PCMs) undergoing Solid-solid phase transitions.**

The Output from this deliverable D3.1 will be crucial for Task 3.2, related to the development and characterization of the refractory materials, and Task 3.3, focused on the development and characterization of the PCM.

2. General methodology

To carry out the preliminary selection of potential materials that will compose HEATERNAL, the following KPIs defined in WP2 (D2.1) have been considered, which are directly related to material selection.

Table 1: HEATERNAL KPIs from D2.1.

KPI	Description
[KPI#2]	3 novel PCM material formulations with cascading phase transition temperatures from 600 to 900 ºC, enthalpy of phase transition over 150 J/g, stability for more than 1000 h.
[KPI#8]	CAPEX at 20€ per kWh TESS capacity (compared to 30.96 €/kWh for molten salts), 0 €/kWh OPEX for 10 years for IWH recovery, OPEX limited to electricity costs when heat comes from RE.
[KPI#12]	Volume variation <10% maximum from 600–900°C to prevent stress induced cracking.
[KPI#13]	Stable phase change temperature, evolving < 3% over 1000 hours.
[KPI#14]	No p-chemical interactions between PCMs & ceramics after 500 h of immersion tests to prevent damage to ceramics and ensure a long lifetime.
[KPI#17]	Unit production process shall be able to use existing /commercially viable processes for refractory manufacturing (MRL of 9-10). Ability to begin Unit mass production via existing processes within 2 months following demonstration.
[KPI#18]	Ability to begin PCM alloy mass production via MRL9-10 processes within 6 months following demonstration. Next-generation TES Unit Manufacturing

KPI#2 is directly related to material selection, however, the other KPIs are taken into consideration regarding price, stability, compatibility, ease of manufacturing and scaling materials with existing processes. The selection of formulations for the refractory will be based on the existing knowledge of the expert members of the consortium. To achieve this, CALD and TCID will select refractory materials from their existing formulations, aiming to minimize porosity and wettability.

The selection of metal alloys, primarily based on aluminium and/or copper, will utilize the CALPHAD method for calculating phase diagrams (CICe) and extensive literature reported in the bibliography regarding these materials (CEA).

3. Refractory Materials

3.1 Interplay Between Refractory Materials and Metal Alloys: An Overview

The corrosion of refractory materials is observed in several fields of application, including but not limited to iron and steel. The refractories used in the aluminium industry can also undergo severe corrosion due to reactions with molten aluminium depending on the conditions (temperature, type of alloy, …) and on the refractory selection (type of bond, additives, etc.). The most suitable refractory material systems are based on the alumina-silica system, in particular high-alumina or mullite containing castables. Variations in purity, porosity and the kind of bonding will lead to different corrosion rates.

First, the kind of raw material determines the microstructure and type of glassy phase, second, the type of bonding provides not only mechanical strength until ceramic bonding is activated but also contributes to the matrix microstructure by introducing pores. Corrosion reactions occur in contact to molten aluminium alloys where (Al_2O_3+SiO_2) stands for a variety of compositions in the alumina-silica system.

The corrosion process is following different steps and is leading to the structural degradation of the refractory material as follows:

- Wettability: Wetting reactions at the interface between the alloy and the refractory.
- Penetration: Penetration via the open porosity and interconnected pores due to capillarity forces.
- Reaction: Degradation, deterioration, decomposition, and wear are all words used to describe corrosion of refractories. Corrosion involves a combination of different mechanisms, such as dissolution and invasive penetration (diffusion, grain boundary, and stress corrosion), and oxidation-reduction reactions (absorption, desorption, and mass transport phenomena). In fine, this leads to the formation of secondary phases having different physical and chemical properties than the original refractory lining.

In practice, what happens when aluminium is in contact with a silico-aluminate refractory?

There is the contact between liquid aluminium and the refractory material, which introduces problems due to infiltration followed by severe chemical reactions of oxides due to the high affinity of aluminium for oxygen. The oxidation of aluminium is the biggest problem at the interface between liquid metal, refractory and oxygen. This phenomenon is often referred to as corundum growth, according to the following equations (1) and (2):

Equation 1 refers to a direct reduction process (Lanxide Process) leading to the formation of “corundum”. This is in fact not only corundum but a metal/mineral composite - Al+Al_2O_3 with mutually interconnected tridimensional network of Al and Al_2O_3. The alumina from the composite provokes dimensional changes and cracking of the healthy lining; the aluminium penetrates further into the refractory and continues the reduction process. In further extent, structural destruction is observed.

$$\frac{4}{3}Al + 0_2 \rightarrow \frac{2}{3}Al_2O_3 \quad (1) – \text{With presence of oxygen}$$

Equation 2 refers to the reduction of reducible oxides in the refractory. Example with silica which is the most reducible oxide and the most predominant in term of quantity. This also leads to structural damages and the formation of SiO(g).

$$4\,Al + 3\,Si0_2 \rightarrow 2Al_2O_3 + 3\,Si \quad (2)$$ – Inside the refractory

Modern alloys with constituents of silicon, zinc and magnesium contribute to increasing corrosion rate.

3.2 Literature review refractory material-alloy interaction

An intensive literature review has been performed in order to gather as much information as possible regarding the corrosion behaviour of the alloys with the ceramic materials. For example, Fukahori et al. (2016) focused on four Al-Si alloys with different Si concentrations (ranging from 0 to 25 wt %), which were selected as PCM materials and six ceramic materials (Al_2O_3, AlN, S_3N_4, SiC and SiO_2) for corrosion tests[1]. The tests were performed at 1000 °C, for 100 h, in an Ar atmosphere. Each sample was cut after the heat treatment to highlight the interface between the ceramic specimen and the alloy[1]. The ceramics that exhibited corrosion were the Al-Si alloy with the SiC interfaces and the Al-Si alloy with SiO_2 interfaces.

In Figure 1, it is observed that in all samples, Al was found in the SiO_2 substrate. From a thermodynamic point of view, these results are expected since Al has a higher oxygen affinity than Si. In the end, the authors concluded that SiO_2 is not appropriate for use as a structural component of an Al-Si alloy PCM. Furthermore, Figure 2 shows the interface between the Al-Si alloys and the SiC substrate. In this case, carbon was detected on the Al side, indicating that Al carbide was formed:

$$3SiC(s) + 4Al(l) = Al4C3(s) + 3Si(l) \quad (3)$$

Thus, due to the presence of a region where Al and Si activities are locally dissimilar, the corrosion persists.

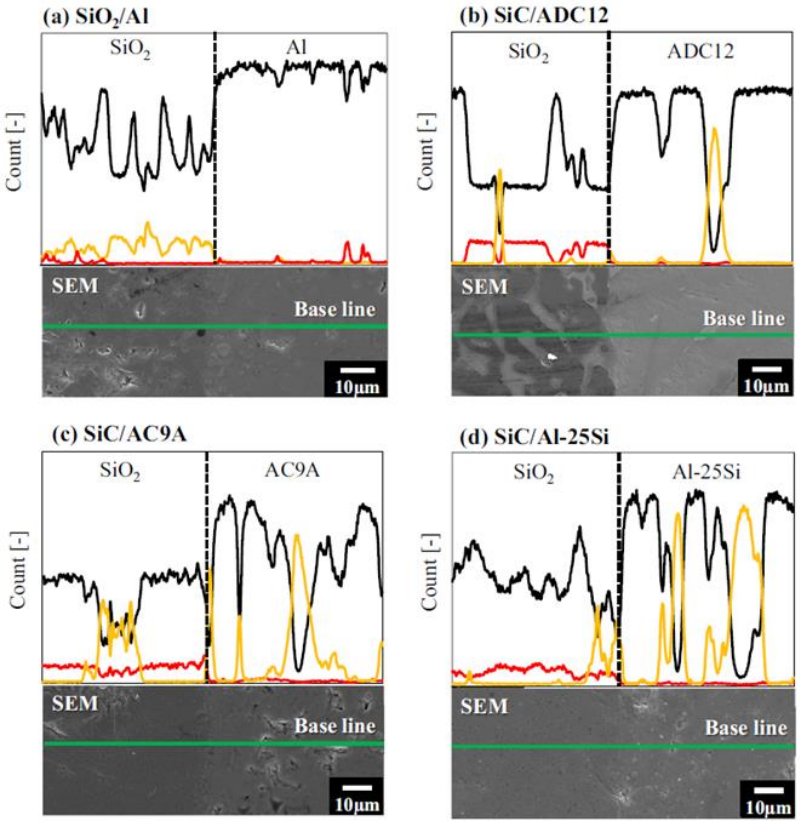

Figure 1: EDS line analyses on the SiO_2 interface carried out by SEM, as reported by Fukafori et. Al (2016)

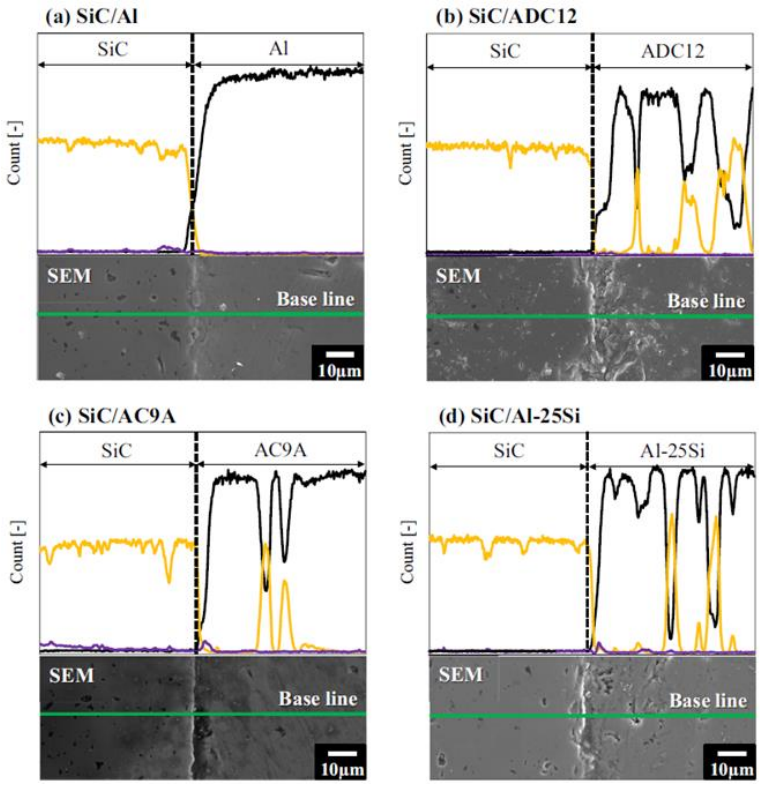

Figure 2: EDS line analyses on the SiC interface carried out by SEM, as reported by Fukafori et. Al (2016)

In the end, the study reported the thermal analysis of Al-Si as a pertinent candidate for high temperature (over 500 °C) applications, showing that Al_2O_3, AlN, and Si_3N_4 ceramic materials presented the best corrosion resistance to the molten Al-Si[1].

Due to the interesting features of the Al-Si alloy used as a PCM, Zhao et al. (2019) conducted experimental studies on the cycling stability and corrosive properties of Al-Si alloys[2]. Therefore, corrosive tests (as well as cycling stability tests) were made on hypoeutectic, eutectic and hypereutectic Al-Si alloys, such as AlSi7, AlSi12, AlSi20 and AlSi30 % wt. The temperature range of 500 – 900 °C was chosen for the cycles charge-discharge.

During the study, Zhao et al. (2019) observed that Al_2O_3 ceramics and AlN ceramics could resist corrosion against molten Al-Si alloys. The mass ratio of Si in Al-Si alloys plays an important role in the corrosion resistance of SiC ceramics against molten Al-Si alloys.[2]

Figure 3 presents the interfaces between Al-Si alloys and ceramic materials. Although BN, Si_3N_4 and ZrO_2 ceramics would react with molten Al-Si alloys, the corrosion behaviour still needs to be further investigated because the reaction products consist of AlN or Al_2O_3, which are corrosion resistant in molten Al-Si alloys[2]. For example, the chemical reaction between AlSi and Si_3N_4 :

$$4Al(l) + Si_3N_4(s) = 4AlN(s) + 3Si \text{ (in Al)}$$

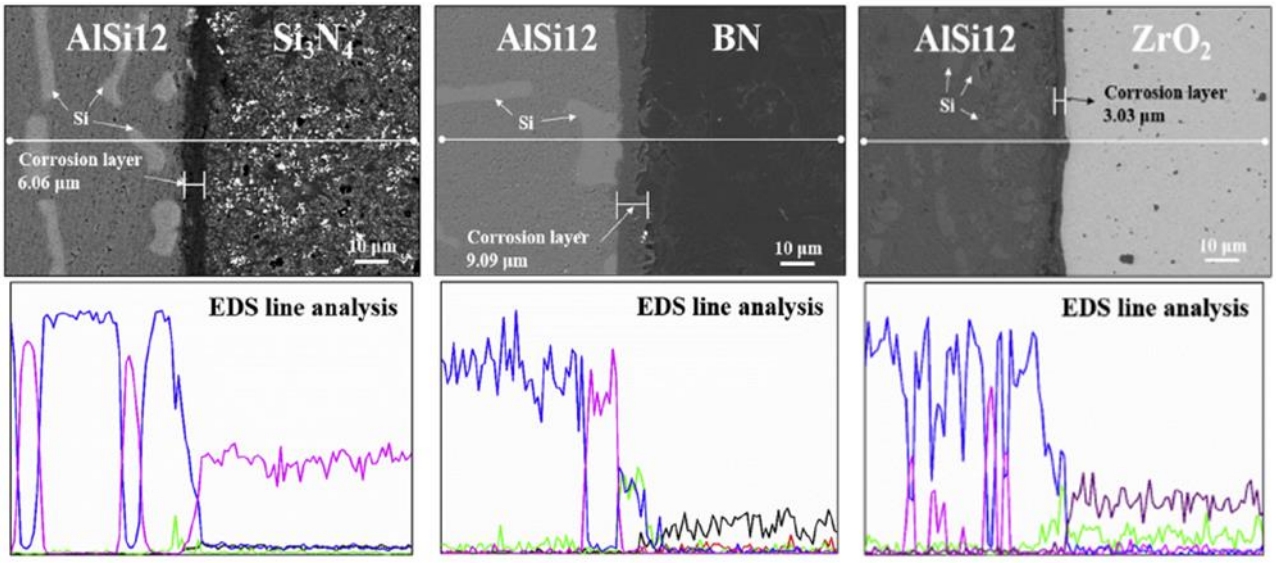

Figure 3: Microstructure of the interfaces Al-Si alloy with Si_3N_4 (left), BN (middle) and ZrO_2 (right) ceramics and EDS line, as reported by Zhao et al. (2019)

Copper based alloys are a weaker reducing agents than Al based alloys, and as a metal may wet and infiltrate oxide-based ceramics poorly. According to the O_2 partial pressure near the PCM, Cu alloys can oxidize and consequently wet the refractories and eventually, at high temperatures, infiltrate the refractories. This mechanism is currently used in the DBC (Direct Bonding Copper) process for mechanically coupling copper to alumina.

In conclusion, due to the high affinity of aluminium towards oxygen, the oxidation of aluminium is the biggest problem, either by direct oxidation or oxido-reduction inside the refractory. Corrosion of refractories by aluminium is more of a chemical nature than of an electrochemical,

Certain parameters promote corrosion:

- A non-appropriate microstructure and composition of the refractory.
- The formation of gases that develop in the pores of the refractory lining (in alkali and aluminium metal (in vapour form).
- The composition of the alloy.
- Temperature.

3.3 Mitigation Strategies for Enhancing Compatibility and Longevity

A firm link between the formed corundum and the refractory material is established. Fortunately, there are ways to control and limit this corrosion phenomenon.

It seems evident that to prevent refractory degradation, a high infiltration resistance against gaseous species, liquid alloys, and slags is crucial. Molten aluminium penetrates pores greater than 0.5µm.

Over the last decades, the development of refractories has led to less permeable refractory solutions:

- High Alumina Bricks (Pore ~ φ :20-30 µm)
- Phosphate Bond Bricks (Pore ~ φ :2-6 µm)
- Conventional Castable (Pore ~ φ :0.8-2 µm)
- Low Cement Castable (Pore ~φ :0.3-0.5 µm)

But this is not enough to face modern and complex aluminium alloys. Therefore, the optimization of the refractory composition is based on using non-wetting additives to reduce metal penetration and stop the reaction.

Barium sulphate ($BaSO_4$) is one of them, among others (CaF_2, AlF_3). However, in operation, the temperature can increase up to 1200 °C, which results in an overheated metal surface and a high-temperature load for the refractory, which can lower the performance. $BaSO_4$ melts at 1580 °C but decomposes before melting between 1100 °C and 1150 °C into barium oxide (BaO) and sulphur dioxide (SO_2). This reaction defines two temperature regimes for the effect of $BaSO_4$ additions to alumina refractories: One below 1100 °C and the other above 1150 °C. In a silica-rich environment, barite decomposes above 900 °C into the barium-alumosilicate, $BaAl_2Si_2O_8$, or even more likely, into a glassy phase.

As previously mentioned, phosphate bonds are one example of several bonding systems, especially for high-temperature applications. Bonding occurs via polycondensation to form $AlPO_4$. The ceramic bonding during sintering replaces the chemical and adhesive bonding by the polyphosphate. Phosphate will also form a high refractory phase with the alumina refractories that help to improve the corrosion resistance.

3.4 Selected Formulations

Two options are considered, which are standard and commercial grades.

One with antiwetting agent: The role of the non-wetting agent namely barium sulphate, will help in reducing the wettability and the porosity, thus limiting the corrosion process, mostly by aluminium. The anti-wetting agents start to degrade above 900°C. The selected product is ALKON CAST MT 90. This is an alumino silicate castable based on high alumina raw material (tabular: sintered alumina).

One with phosphate addition: The role of phosphate provides non wetting properties toward metals in general. Phosphates help to improve the strength and resistance to temperatures above 1200°C. The selected product is CALDE CHEM PB 85. This is an alumino silicate castable based on bauxite raw material.

Table 2: Selected refractory formulations.

Product name	Material Type	Max temperature of use (Measured via Refractoriness Under Load Testing)	Anti Wetting resistance	Main Raw Material	Corrosion resistance	Porosity	Permanent Linear change	Reversible Thermal expansion
ALKON CAST MT 90	Alumino Silicate Monolithcs	1550°C	Up to 1200°C	Tabular alumina	Mostly Aluminium Grade	Porosity size: <0.3µm	0% (800°C) 0% (1200°C)	0.88%
CALDE CHEM PB 85	Alumino Silicate Monolithcs (P bonded)	1400°C	Up to 1400°C	Bauxite	All Metals	Porosity size: 2-6µm	-0.2% (800°C) -0.5% (1200°C)	0.84%

4. Phase Change Materials

4.1 Selection Criteria

Three target temperature ranges are established for the search for PCMs based on the requirements of the Use Cases established in D2.1. Thus, candidates will be sought for the following temperature ranges:

- 550 ºC - 700 ºC
- 700 ºC - 800 ºC
- 800 ºC - 900 ºC

Before delving into the selection of metallic alloys, we will screen out those metals that are initially impediments to meeting the previously established requirements. Taking into account the KPIs defined in Table 1, the selection criteria include the parameters of melting point (range of temperature criteria), latent heat (energy storage capacity criteria), price (cost criteria), and vapour pressure (stability criteria) (see Figure 4).

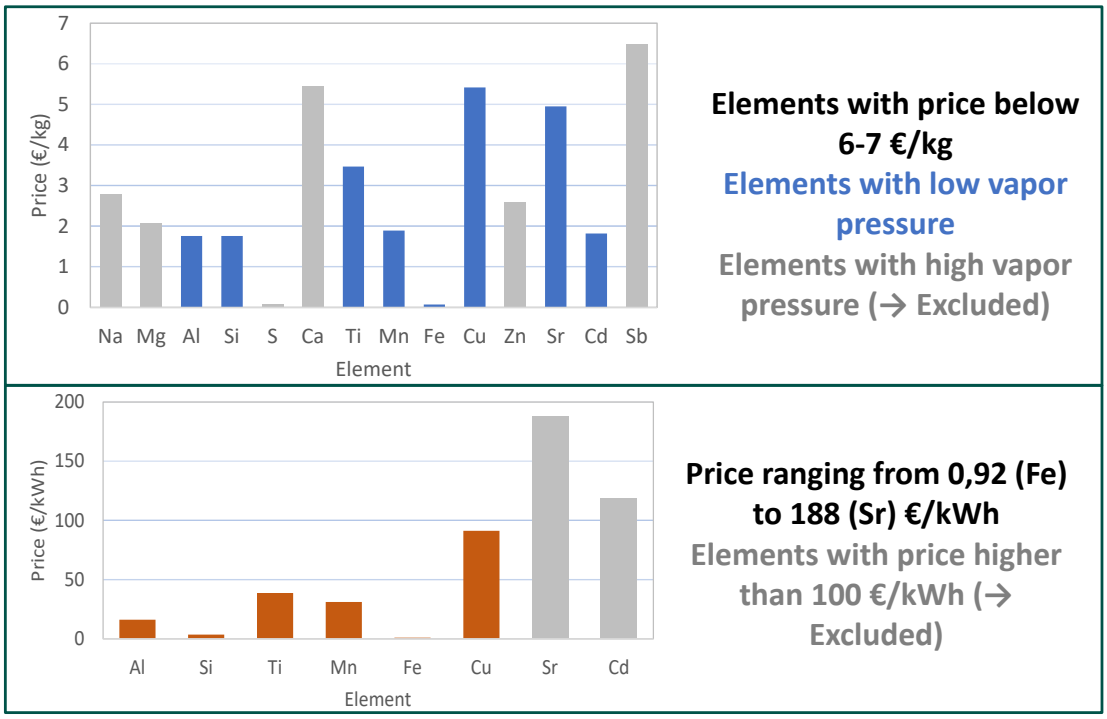

Figure 4: Various metals were eliminated due to their high cost or vapour pressure(grey). Potential candidate metals for alloys are displayed in in blue (above) and orange (below).

Based on stability and cost, the selected metals to evaluate are **Al, Cu, Fe, Si, Mn and Ti and their alloys.**

4.2 CALPHAD calculations (FACTsage)

Alloys primarily consisting of a combination of 6 elements (Al-Cu-Fe-Mn-Si-Ti) were explored using a simultaneous approach involving a comprehensive literature search and CALPHAD calculations.

Binary and ternary phase diagrams are also calculated using FactSage Thermochemical Software and Databases, using FTLITE, FACTPS, ELEM, SGTE and FS-STEL thermochemical databases[3]. Calculations are performed over the full range of compositions and temperatures. The output diagrams allow us to identify Liquidus projection and Invariant points (composition and temperature). Priority is given to those invariant points corresponding to eutectic and peritectic reactions. FactSage is then used to predict the expected enthalpy (ΔH) of fusion for the points of interest.

FactSage can offer theoretical results regarding the thermophysical characteristics, however, discrepancies between the results and literature have been observed. For example, in the case of the ternary diagram Al-Si-Cu, the copper-rich corner noted from the literature was compared with three databases (FT-lite, FS-stel and SGTE) using FactSage 8.3[4] (see Figure 5 and Figure 6). As can be observed, the copper-rich corner shows slight differences compared to the experimental results.

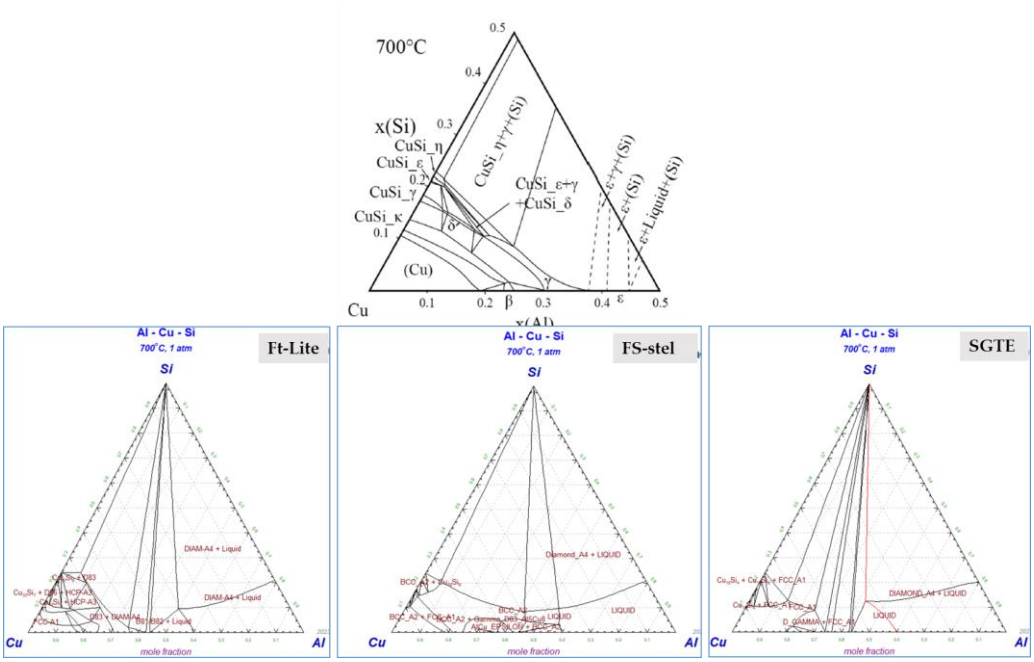

Figure 5: Isothermal section of phase diagram Al-Cu-Si at 700 °C reported by Zobac et al (2020), (top image), compared with FactSage databases (bottom images

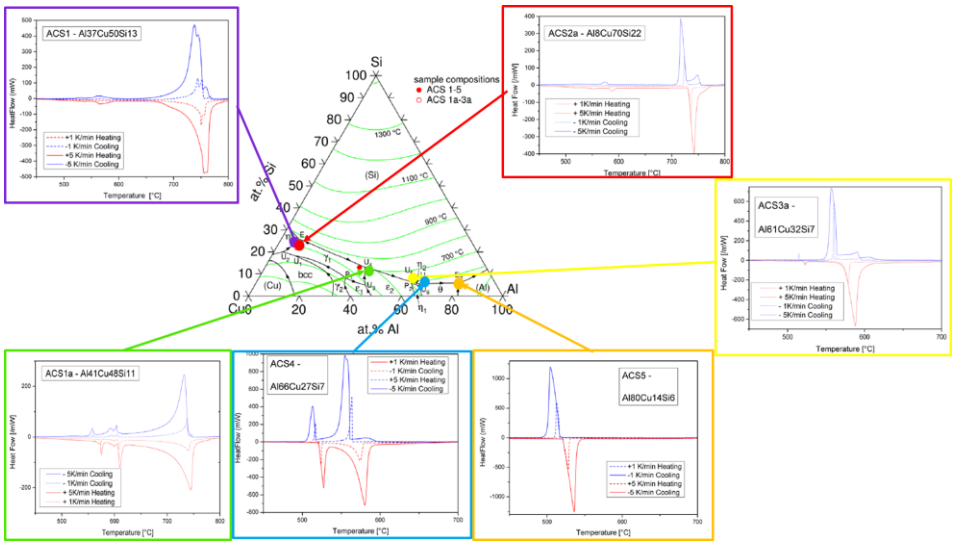

Figure 6: Calculated liquidus projection with DSC curves for the ternary alloys, as reported by Hallstedt et al. (2016)[4]

Therefore, for binary alloys, the CALPHAD method, using FACTSage is a good choice. However, results should be cross-referenced with available literature (experimental results) for ternary systems.

4.3 Synthesis methodology

Each of the identified candidate metal alloys was cross-referenced to literature sources, and then each metal alloy was synthesized as follows:

4.3.1 Direct melting under inert atmosphere (CICe)

The metals were ordered from HMW Hauner GmbH & Co. KG Gewerbering 36 (Table 3)

Table 3: List of metals used in the preliminary synthesis of PCMs.

Metal	HMW Hauner. Art.No.	Mass, g	Shape (available and easy to work with)	Price, Eur
Al 99.999%	1376082	300	Granules <2 mm	502.89
Cu 99.999%	2976123	500	Granules <5 mm	421.79
Si 99.999%	1476013	100	Granules 1 – 20 mm	96.25
Fe 99.99+%	2674050	100	Granules <5 mm	129.78
Mn 99.8%	2571037	100	Flakes <2 mm	74.16

All metals were stored within an argon glovebox to prevent oxidation. The metals were weighed to form ~2 grams of total material (+-0.05 g accuracy). The resulting mixture was then pressed into a pellet using a pressure of 10 tonnes in a uniaxial press. The pellet was placed in a graphite crucible and inside a muffle furnace. Flowing N_2 (6L/ min) was applied to keep the metal under inert conditions and prevent oxidation.

The alloy pellet was heated (10 °C/min) to various temperatures (approximately > 100 °C above the temperature of the lowest melting point in the alloy) and then held in an isothermal state for 3 hours. After

cooling, the alloy was weighed to clarify that no mass was lost (< 1 %). A small piece of the alloy was cut out from the centre of the sample and placed in an alumina crucible to perform simultaneous thermal analysis (STA) using a (NETZCH Jupiter 443 STA).

4.3.2 Induction melting CEA

Repetitive tests regarding the synthesis of the metals have been made in the laboratory using a resistance furnace Nabertherm under air. Before and after the melting process, the samples were weighted and analysed. The first test consisted of melting $AlSi_{12}$ powder (eutectic point, see Figure 12). From the start, two thermocouples have been introduced, one in the furnace and one in the sample, to record and have a better view of the temperatures over time.

Figure 7: Sample of AlSi12 powder, heated up to 800°C, in alumina crucible

The melting protocol consisted of heating up until 800 °C for 4 hours ($\Delta T/t$=3°C/min) and maintaining this temperature for 4 hours. In the end, it was observed that the powder did not fuse completely, highlighting a problem of oxidation of the sample (Figure 7). Thus, additional tests have been performed, such as melting the samples at a higher temperature (900 °C) under N_2 atmosphere and adding a Titanium lid to trap the oxygen molecules. However, the results were still unsatisfying.

Complementary to the synthesis protocol for $AlSi_{12}$, binary Cu-Si alloys have also been considered to be included in the protocol analysis due to the interesting results reported by Hallstedt et al., (2016)[4]. For this, two points from the binary diagram (Figure 8) have been chosen for doing tests in the laboratory, respectively Cu87.75Si12.25 (wt%) (CS4) and Cu83.69Si16.31 (wt%) (CS5) points.

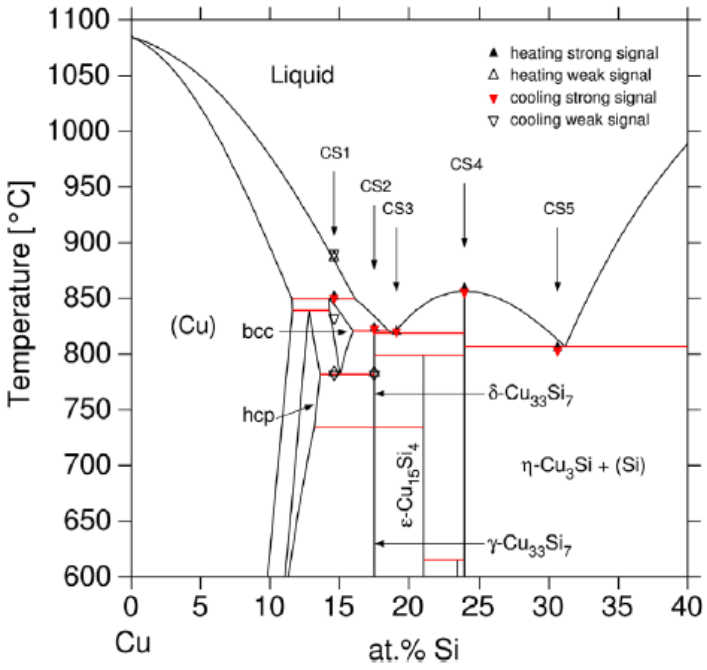

Figure 8: Phase diagram Cu-Si, calculated Hallstedt et. al [4]

For this, an arc melting furnace and an induction furnace were used to melt the alloys. The macro-observation of the Cu87.75Si12.25 (wt%) samples indicates that better results were achieved through inductive melting. The material exhibits a homogeneous structure, as depicted in Figure 9.

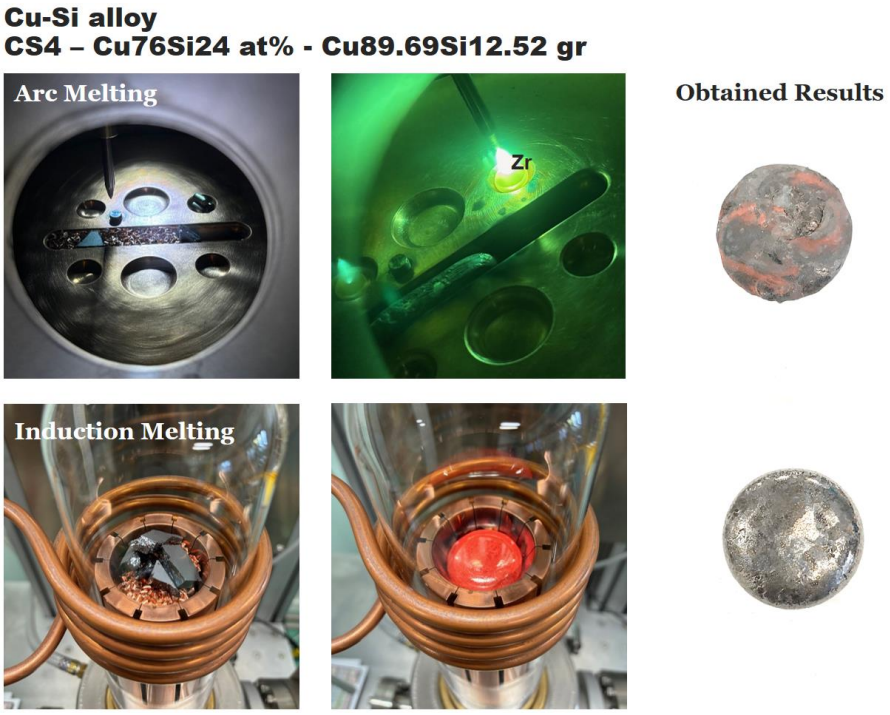

Figure 9: Cu87.75Si12.25 (wt%) (alloy, melted by arc-melting furnace and by induction, with the final results

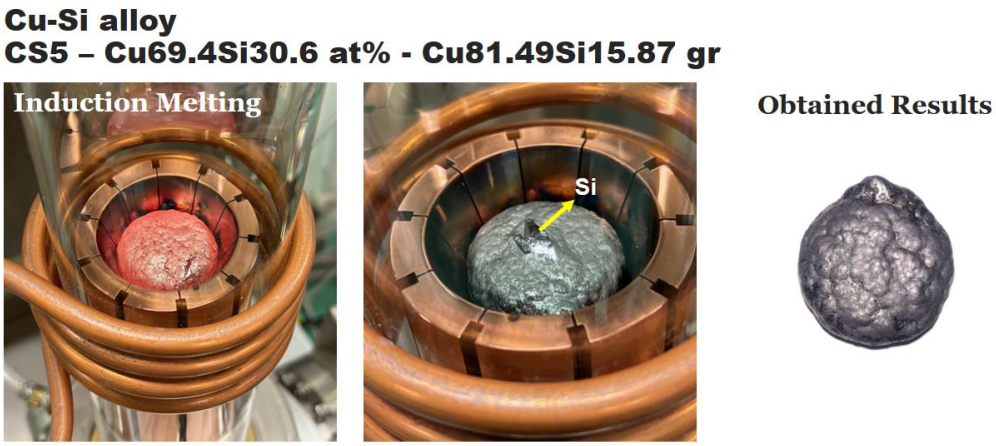

Figure 10 Cu83.69Si16.31 (wt%) alloy, melted by induction.

Due to the results obtained from the first Cu alloy, Cu83.69Si16.31 wt% was melted as well, by induction method. However, the alloy behaved differently during solidification, highlighting a “cauliflower” morphology, as can be observed in Figure 10. From the first melting it was still observed the presence of Si block, therefore Cu83.69Si16.31 was melted multiple times, in order to obtain a homogeneous structure.

Future analysis regarding the samples Cu83.69Si16.31 wt% and Cu87.75Si12.25 (wt%) are planned for the following months. To start with, CEA results will be compared to CIC synthesized material (Figure 16). Hence, little pieces of the material will be sent to CICe for DSC measurements, and the new results will be compared with the present ones (Figure 16). In addition, CEA team will make Dilatometry (CTE) analysis and SEM-EDX observations of the Cu-Si alloys.

5. PCM Candidate selection

5.1 Candidates for 550 ºC - 700 ºC

5.1.1 Pure Al

The first candidate that appears in the lower temperature range is aluminium. It is a pure metal with a high energy density. Its main thermophysical properties are presented in **Table 4.**

Table 4: Aluminium thermophysical properties, as reported in literature [5,6].

Aluminium Properties					
Heat Capacity (Solid) J/gK	Temperature Phase transition °C	Heat of Fusion J/g	Density g/cm^3	Thermal Conductivity W/m/k	Volume expansion (10^{-6}/K)
0.9	660	395	2.7	273	80.1

For aluminium, stability issues, in addition to its oxidation, are not expected. It has a melting point of 660 ºC with a phase change enthalpy of 397 J/g. It meets all the criteria established in KPI#2. The Simultaneous thermal analysis (STA) of pure Al is shown in Figure 11, where its melting point and latent heat are confirmed.

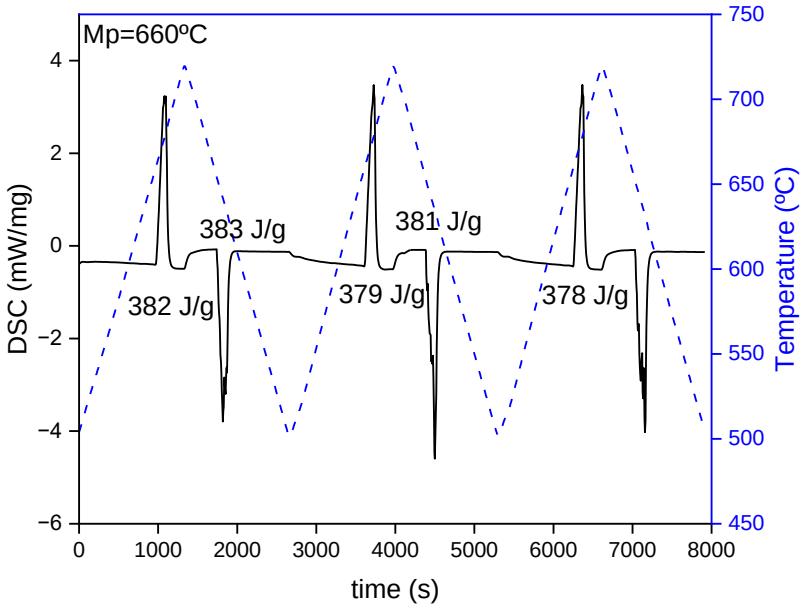

Figure 11: Simultaneous thermal analysis characterization of Aluminium.

5.1.2 Binary $Al_{87.4}$ – $Si_{12.6}$

A binary system consisting of aluminium and silicon was selected due to the high enthalpy of 560 J/g[8] corresponding to its eutectic composition (Figure 12). This is well established system in the literature and forms an eutectic alloy at 12.6 wt% of silicon.[9] Melting temperature and latent heat of this alloy show little change over 1000 thermal cycles[10]. Moreover, the reported thermal conductivity remains high at over 182 W $m^{-2}K^{-1}$ at a temperature of 500 °C, proving effective performance for fast charging and discharging [10]. This alloy is an ideal candidate to fulfil the criteria of KPI#2.

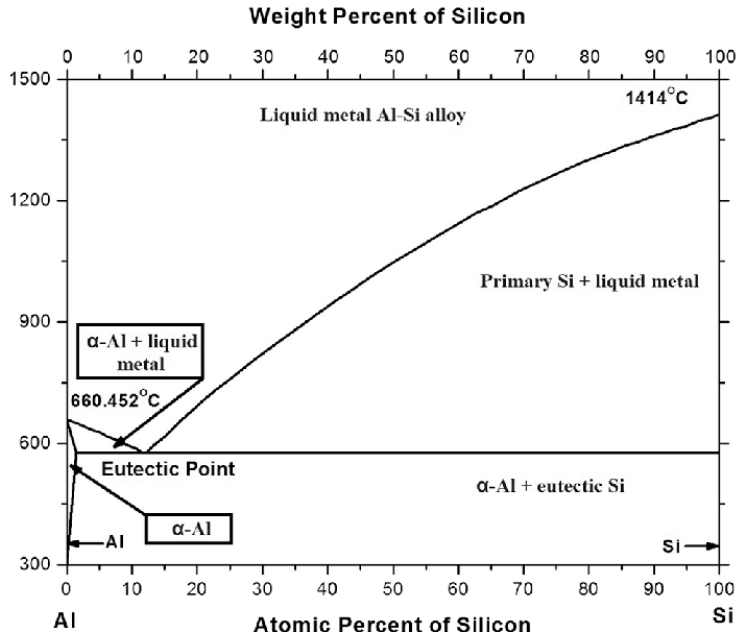

Figure 12 : Phase diagram of Al-Si binary alloy as reported by Z. Wang et al., (2017)

The STA results for the $Al_{12.6}$-$Si_{83.6}$ binary are presented in Figure 13, where a single-phase change is observed in melting and solidification, suggesting successful synthesis. The enthalpy of fusion was measured to be 529 – 560 J/g which corresponds with the 560 J/g measured by X. Wang et al., (2006).

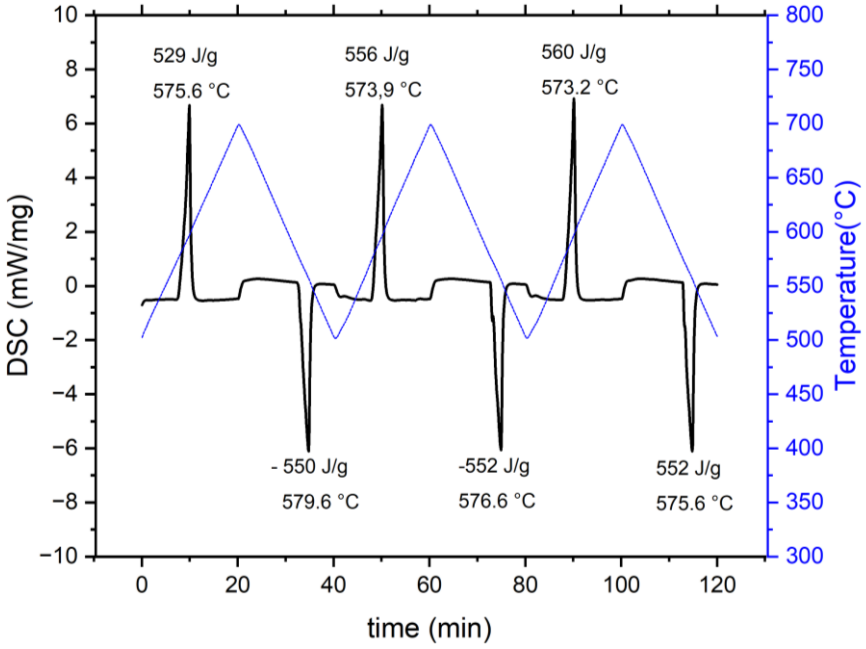

Figure 13: Thermal characterization of a composition of 12.6 wt.% Si and 88.4 wt.% Al T=700°C, t_{iso}=3 hours, (∆T/t)=10°C/min.

One of the interesting characteristics of the Al-Si binary system is that the content of Si can be adjusted, so that the enthalpy can be kept high while the coefficient of thermal expansion (CTE) can be potentially reduced when increasing the Si content. This reduction of the CTE can be beneficial from the thermomechanical point of view once the metal alloy and the refractory material are combined.

5.1.3 Solid-solid PCM (Li_2SO_4 - Na_2SO_4)

In addition to metallic alloys, PCMs with solid-solid phase transitions offer several advantages over solid-liquid systems, such as the inherent property of operating in a solid state and exhibiting low CTE. Within the specified temperature range, the Li_2SO_4 - Na_2SO_4 binary system emerges as a candidate.

In the phase diagram of this system (Figure 14), two compositions present high interest: eutectoid composition (Mole fraction of Li_2SO_4 = 0.79), and stoichiometric composition (mole fraction of Li_2SO_4 = 0.5). According to their thermal properties (Figure 15), the stoichiometric composition (LNS), with a solid transition at 526 ºC and a latent heat of 157 J/g, is the selected material for further experiments.

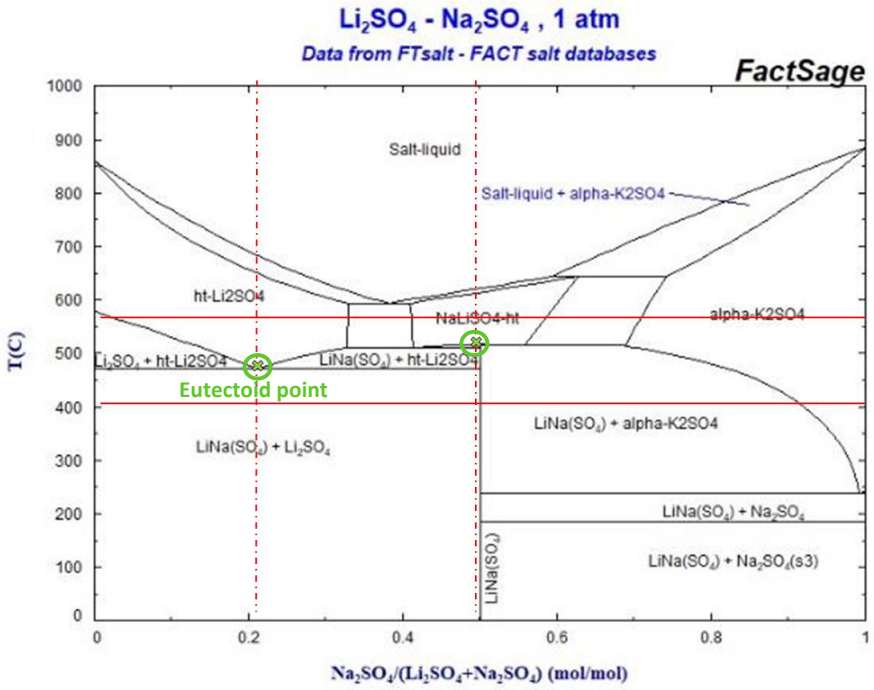

Figure 14: Lithium-Sodium sulphate phase diagram

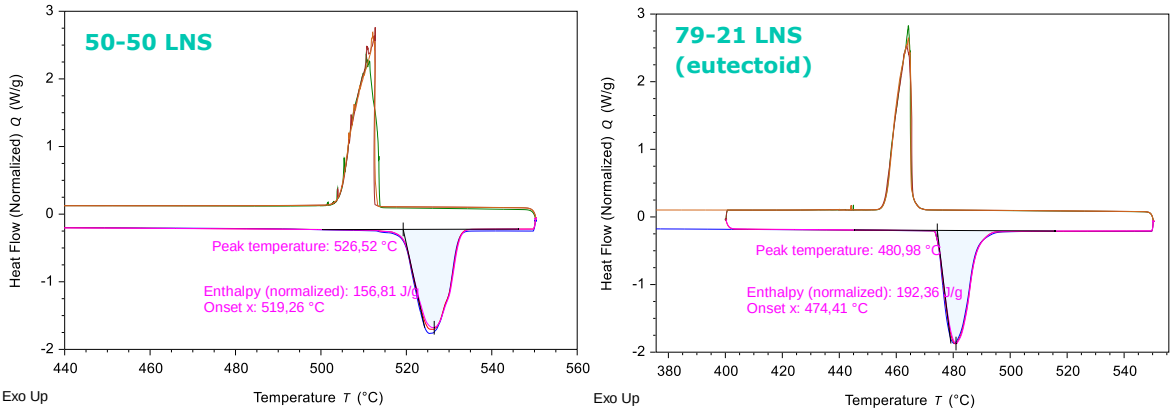

Figure 15: DSC results for stoichiometric and eutectoid compositions (Lithium-Sodium sulphate system).

5.2 Candidates for 700 ºC - 800 ºC

The binary composition of copper and silicon was investigated (Figure 16). The high enthalpy of this Cu-Si alloy makes it an ideal candidate. The results from this binary are expected to provide information on the closely related ternary eutectic composition for the Al-Cu-Si system.

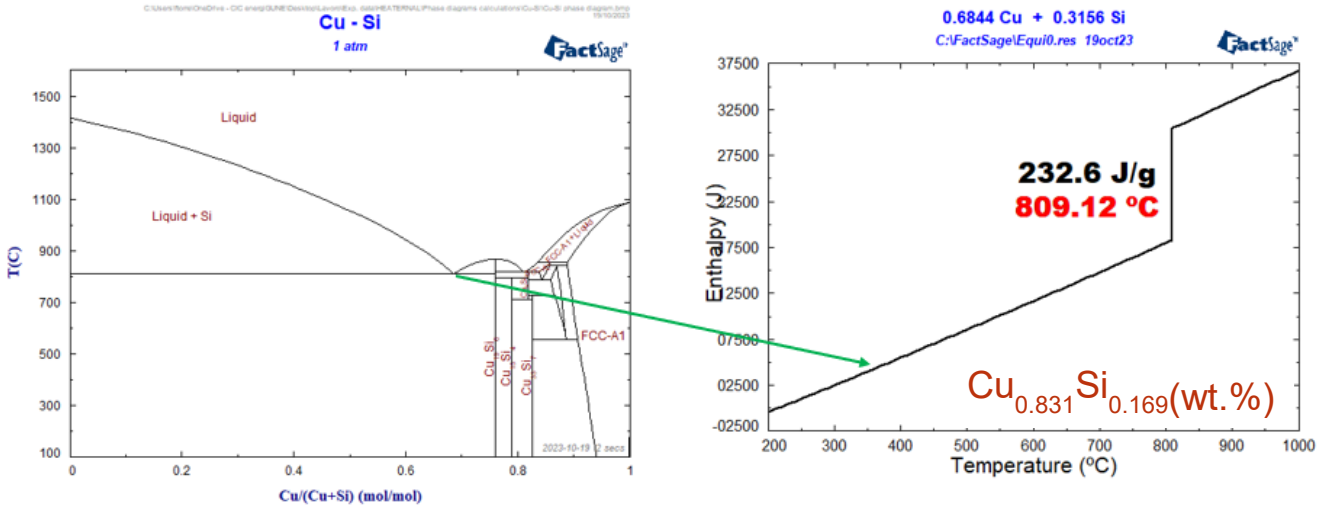

Figure 16: CALPHAD calculations performed using FactSage for the binary phase diagram Cu-Si.

The Al-Cu-Si ternary system was additionally identified as a potential source of candidates where CALPHAD calculations resulted in two potential compositions (Figure 17). The calculated results were cross-referenced in the literature with a recent paper by Hallstedt et al., (2016) (Table 5).

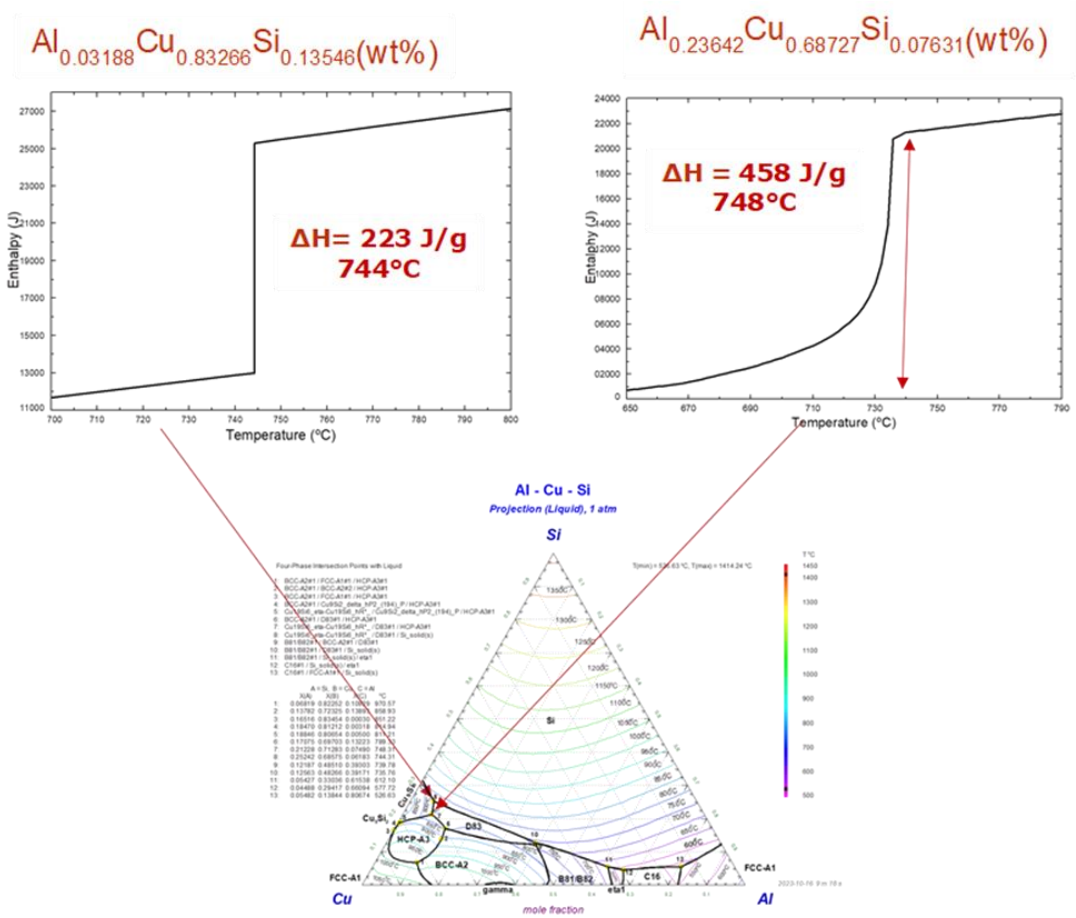

Figure 17: CALPHAD calculations performed using FactSage for the ternary alloy Al-Cu-Si highlighting two invariant points in the Cu-Si-Al system.

Table 5: Predicted invariant points for compositions in the Al-Cu-Si system [HS] is the experimental results of Hallstedt et al., (2016) and where [FS] is the results from FactSage calculations.

#	Composition wt%	Expected Reaction	Temperature (°C)	Enthalpy (J/g)
Cu-Si	$Cu_{0.83}Si_{0.17}$	Liquid-> η-Cu_3Si+(Si)	809[FS] 803[HS]	233 [FS] 128 [HS]
Al-Cu-Si Eutectic	$Al_{0.032}Cu_{0.83}Si_{0.14}$	L -> η_S+γ_1+(Si)	748 [FS] 750[HS]	236 [FS] 141 [HS]
Al-Cu-Si Peritectic	$Al_{0.24}Cu_{0.69}Si_{0.08}$	L+γ_1- >(Si)+ε_2	744 [FS] 740[HS]	458 [FS] 264[HS]

5.2.1 Cu_{83}–Si_{17} (wt%) Binary

The preliminary STA results for the Cu-Si binary are presented in Figure 18, where a single-phase change is observed in melting and solidification, suggesting successful synthesis. These preliminary enthalpy measurements lie in the 138.7 - 170.1 J/g range, between the calculated value (233 J/g) and the literature experimental value (128 J/g). The onset temperature is between 800°C – 805 °C, which corresponds well with 803 °C measured by Hallstedt et al., (2016).

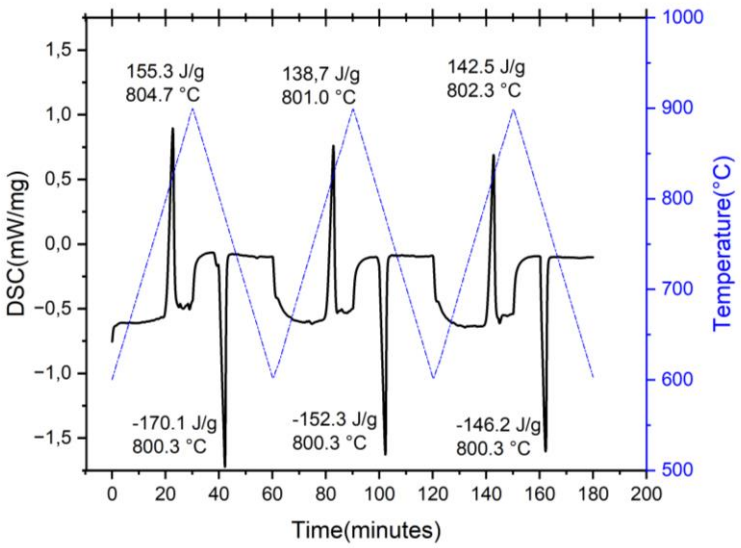

Figure 18: STA results of 83.0 wt.% Si and 17.0 wt.% Cu T= 1100 °C, t_{iso} = 3 hours, (∆T/t) = 10 °C/min.

5.2.2 Al_{24}-Cu_{69}-Si_8 (wt%) peritectic

The preliminary STA results for the Al_{24}-Cu_{69}-Si_8 (wt%) peritectic are presented in (Figure 19). A single peak is observed, which suggests successful synthesis. The enthalpy of fusion 236 – 295 J/g is similar to those measured by Hallstedt et al. (2016), however, it falls shy of the 458 J/g predicted by FactSage.

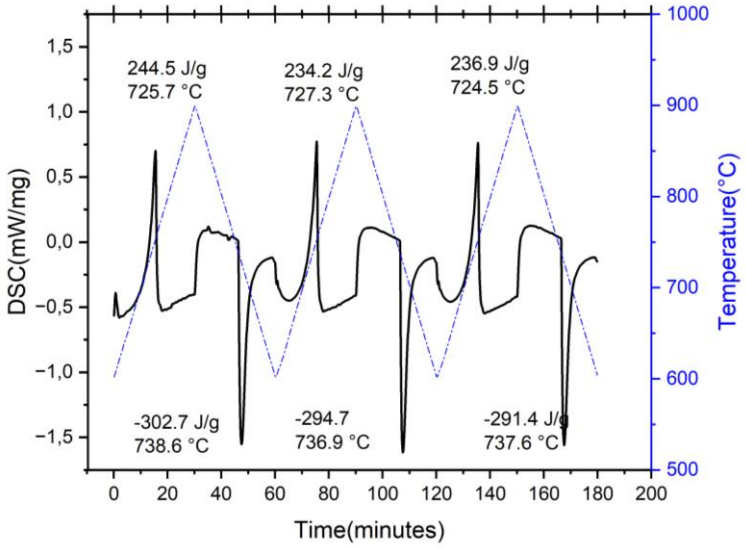

Figure 19: STA results of Al_{24}-Cu_{69}-Si_8 (wt%) – peritectic, T=1100°C, t_{iso} = 3 hours, ($\Delta T/t$) = 10 °C/min.

5.2.3 Al_3-Cu_{13}-Si_{83} (wt%)– eutectic

Preliminary STA results (Figure 20) show a melting point that is very close to that of the binary system (798.2 °C). This indicates that the synthesis procedure is ineffective and needs to be performed at a higher temperature. The synthesis procedure for this material will be optimized by applying the synthesis protocol carried out at CEA (inductive melting).

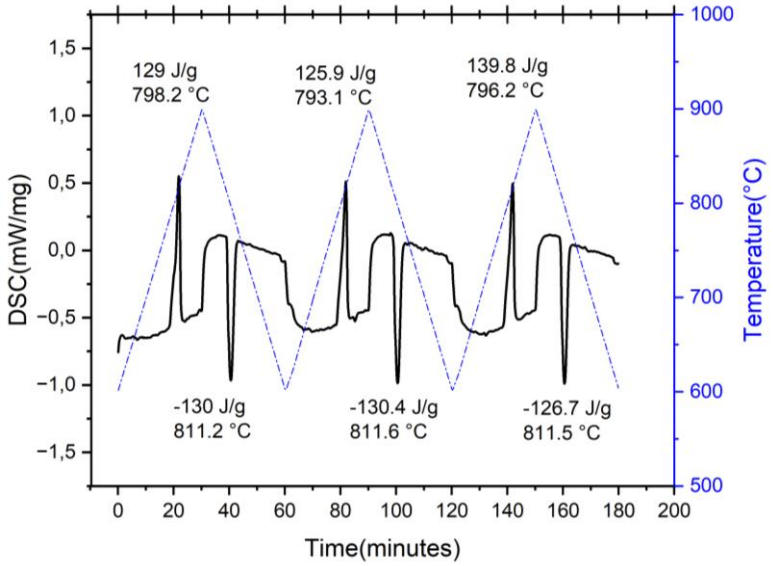

Figure 20: STA results of a composition of Al_3-Cu_{13}-Si_{83} – eutectic, T= 900 °C, t_{iso}= 3 hours, ($\Delta T/t$) = 10 °C/min.

5.3 Candidates for 800 ºC – 900 ºC

5.3.1 Al_{38}-Si_{26}-Fe_{35} (wt%) eutectic

The eutectic alloy $Al_{38.2}Si_{26.4}Fe_{35.4}$ (wt%) has been previously reported by Lee et al., 2011 as an invariant point, as well as on the patent application[12]. The preliminary STA results for the ternary $Al_{38.2}Si_{26.4}Fe_{35.4}$ display one peak on melting at ~800 – 829 °C and two peaks on solidification (Figure 21). These results suggest that the synthesis of the alloy requires optimization; however, it is noteworthy that the enthalpy of fusion, even in a non-optimized and fully formed composition, remains high (ranging from 260 to 272 J/g). Consequently, we consider it a promising candidate for further experiments.

The synthesis of this alloy will be further revised based on CEA and CICe new synthesis protocols; however, in the high-temperature range this alloy fulfils the criteria of KPI#2.

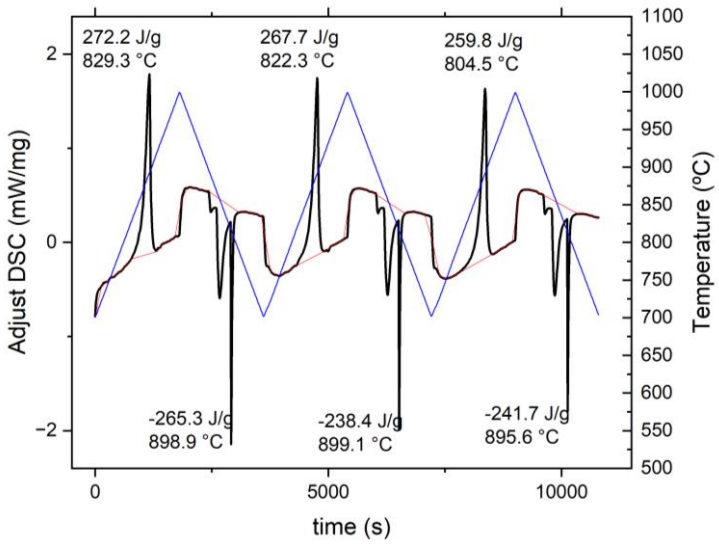

Figure 21: STA results of $Al_{38.2}Si_{26.4}Fe_{35.4}$ – eutectic, T= 1100 °C, tiso= 3 hours, (ΔT/t) = 10 °C/min

5.4 Table of selected PCMs

The final candidate list of PCMs under investigation is presented below (Table 6).

Table 6: Summary of selected materials and results, including preliminary thermal characterisation and experimental results from the literature, [13][D],FACTSAGE[FS],[4][HS],[8][W] and preliminary measurements by CICenergiGUNE [CICe]

#	Composition wt%	Temperature (°C)	Enthalpy (J/g)
Al	Al 100%	660	397
Al-Si	$Al_{12.6}$-$Si_{83.6}$	560[W] 574[CICe]	560[W] 529-560[CICe]
LNS	$LiNaSO_4$ (stoichiometric)	515	318 [D]
Cu-Si	$Cu_{0.83}Si_{0.17}$	809[FS] 803[HS] 800-804[CIC]	233 [FS] 128 [HS] 150-170[CICe]
Al-Cu-Si Eutectic	$Al_{0.032}Cu_{0.83}Si_{0.14}$	748 [FS] 750[HS] 790-811[CIC]	236 [FS] 141 [HS] 125-130[CICe]
Al-Cu-Si Peritectic	$Al_{0.24}Cu_{0.69}Si_{0.08}$	744 [FS] 740[HS] 725-735[CICe]	458 [FS] 264[HS] 236 – 295[CICe]
Al-Si-Fe-	$Al_{38.2}Si_{26.4}Fe_{35.4}$	804-890[CICe]	238-260[CICe]

6. Conclusion

This report gathers the formulations for refractories (Table 2) and PCMs (Table 6) chosen as candidates for the composite intended to be the core of the HEATERNAL TES system.

These materials will continue development and characterization in upcoming tasks. Refractory materials will be used in Task 3.2, involving in-depth characterization and evaluating two processing approaches for optimized geometries, maximizing heat transfer and thermal storage density.

Meanwhile, the selected PCMs will undergo further evolution in Task 3.3, aimed at optimizing and defining the manufacturing protocols for these metal alloys. Additionally, material characterization will be completed to support future modeling of these composites.

The materials selected here meet the project requirements, offering diverse alternatives for each temperature range and energy densities exceeding those specified in the KPIs (150 J/g). Furthermore, the refractory formulations have been specifically chosen to work with metal alloys, minimizing the expectation of dramatic chemical incompatibilities. The long-term compatibility of PCMs/refractories will be thoroughly evaluated in Task 3.4.

Ultimately, the list of candidate PCMs remains open for potential discoveries during the project's progress.

7. References

(1) Fukahori, R.; Nomura, T.; Zhu, C.; Sheng, N.; Okinaka, N.; Akiyama, T. Thermal Analysis of Al-Si Alloys as High-Temperature Phase-Change Material and Their Corrosion Properties with Ceramic Materials. *Appl Energy* **2016**, *163*, 1–8. https://doi.org/10.1016/j.apenergy.2015.10.164.

(2) Zhao, Y.; Liu, H. B.; Zhao, C. Y. Experimental Study on the Cycling Stability and Corrosive Property of Al-Si Alloys as Phase Change Materials in High-Temperature Heat Storage. *Solar Energy Materials and Solar Cells* **2019**, *203*, 110165. https://doi.org/10.1016/J.SOLMAT.2019.110165.

(3) *FactSage.com*. https://factsage.com/ (accessed 2023-12-12).

(4) Hallstedt, B.; Gröbner, J.; Hampl, M.; Schmid-Fetzer, R. Calorimetric Measurements and Assessment of the Binary Cu–Si and Ternary Al–Cu–Si Phase Diagrams. *CALPHAD* **2016**, *53*, 25–38. https://doi.org/10.1016/j.calphad.2016.03.002.

(5) Khare, S.; Dell'Amico, M.; Knight, C.; McGarry, S. Selection of Materials for High Temperature Latent Heat Energy Storage. *Solar Energy Materials and Solar Cells* **2012**, *107*, 20–27. https://doi.org/10.1016/J.SOLMAT.2012.07.020.

(6) Soldi, L.; Laplace, A.; Roskosz, M.; Gossé, S. Phase Diagram and Thermodynamic Model for the Cu-Si and the Cu-Fe-Si Systems. *J Alloys Compd* **2019**, *803*, 61–70. https://doi.org/10.1016/J.JALLCOM.2019.06.236.

(7) Hidnert, P.; States., U. *Thermal Expansion of Aluminum and Various Important Aluminum Alloys*; Scientific Papers of the Bureau of Standards ;no. 497; U.S. Dept. of Commerce, Bureau of Standards : U.S. Govt. Print. Off.: Washington, D.C., 1925.

(8) Wang, X.; Liu, J.; Zhang, Y.; Di, H.; Jiang, Y. Experimental Research on a Kind of Novel High Temperature Phase Change Storage Heater. *Energy Convers Manag* **2006**, *47* (15–16), 2211–2222. https://doi.org/10.1016/j.enconman.2005.12.004.

(9) Wang, Z.; Wang, H.; Li, X.; Wang, D.; Zhang, Q.; Chen, G.; Ren, Z. Aluminum and Silicon Based Phase Change Materials for High Capacity Thermal Energy Storage. *Appl Therm Eng* **2015**, *89*, 204–208. https://doi.org/10.1016/j.applthermaleng.2015.05.037.

(10) Wang, Z.; Wang, H.; Yang, M.; Sun, W.; Yin, G.; Zhang, Q.; Ren, Z. Thermal Reliability of Al-Si Eutectic Alloy for Thermal Energy Storage. *Mater Res Bull* **2017**, *95*, 300–306. https://doi.org/10.1016/j.materresbull.2017.07.040.

(11) Lee, S.; Kim, B.; Lee, S. Prediction of Solidification Paths in Al-Si-Fe Ternary System and Experimental Verification: Part I. Fe-Containing Hypoeutectic Al-Si Alloys. In *Materials Transactions*; 2011; Vol. 52, pp 1053–1062. https://doi.org/10.2320/matertrans.M2010422.

(12) 2014 US20140109895A1.

(13) Doppiu, S.; Dauvergne, J. L.; Serrano, A.; del Barrio, E. P. The Li2SO4–Na2SO4 System for Thermal Energy Storage. *Materials 2019, Vol. 12, Page 3658* **2019**, *12* (22), 3658. https://doi.org/10.3390/MA12223658.


HEATERNAL